

An artificial placenta type microfluidic blood oxygenator with double-sided gas transfer microchannels and its integration as a neonatal lung assist device

Mohammadhossein Dabaghi, Gerhard Fusch, Neda Saraei, Niels Rochow, John L. Brash, Christoph Fusch, and P. Ravi Selvaganapathy

Citation: *Biomicrofluidics* **12**, 044101 (2018); doi: 10.1063/1.5034791

View online: <https://doi.org/10.1063/1.5034791>

View Table of Contents: <http://aip.scitation.org/toc/bmf/12/4>

Published by the American Institute of Physics



An artificial placenta type microfluidic blood oxygenator with double-sided gas transfer microchannels and its integration as a neonatal lung assist device

Mohammadhossein Dabaghi,¹ Gerhard Fusch,² Neda Saraei,³
 Niels Rochow,² John L. Brash,^{1,4} Christoph Fusch,^{1,2,5}
 and P. Ravi Selvaganapathy^{1,3}

¹School of Biomedical Engineering, McMaster University, Hamilton, Ontario L8S 4L7, Canada

²Department of Pediatrics, McMaster University, Hamilton, Ontario L8S 4L7, Canada

³Department of Mechanical Engineering, McMaster University, Hamilton, Ontario L8S 4L7, Canada

⁴Department of Chemical Engineering, McMaster University, Hamilton, Ontario L8S 4L7, Canada

⁵Paracelsus Medical University Salzburg, Department of Pediatrics, University Hospital Nuremberg, Nuremberg, Germany

(Received 12 April 2018; accepted 5 June 2018; published online 3 July 2018)

Preterm neonates suffering from respiratory distress syndrome require assistive support in the form of mechanical ventilation or extracorporeal membrane oxygenation, which may lead to long-term complications or even death. Here, we describe a high performance artificial placenta type microfluidic oxygenator, termed as a double-sided single oxygenator unit (dsSOU), which combines microwire stainless-steel mesh reinforced gas permeable membranes on both sides of a microchannel network, thereby significantly reducing the diffusional resistance to oxygen uptake as compared to the previous single-sided oxygenator designs. The new oxygenator is designed to be operated in a pumpless manner, perfused solely due to the arterio-venous pressure difference in a neonate and oxygenate blood through exposure directly to ambient atmosphere without any air or oxygen pumping. The best performing dsSOUs showed up to $\sim 343\%$ improvement in oxygen transfer compared to a single-sided SOU (ssSOU) with the same height. Later, the dsSOUs were optimized and integrated to build a lung assist device (LAD) that could support the oxygenation needs for a 1–2 kg neonate under clinically relevant conditions for the artificial placenta, namely, flow rates ranging from 10 to 60 ml/min and a pressure drop of 10–60 mmHg. The LAD provided an oxygen uptake of 0.78–2.86 ml/min, which corresponded to the increase in oxygen saturation from $57 \pm 1\%$ to 93%–100%, under pure oxygen environment. This microfluidic lung assist device combines elegant design with new microfabrication methods to develop a pumpless, microfluidic blood oxygenator that is capable of supporting 30% of the oxygen needs of a pre-term neonate. Published by AIP Publishing. <https://doi.org/10.1063/1.5034791>

INTRODUCTION

Preterm infants account for about 10% of 4×10^6 total births each year in the United States,¹ which amounts to $\sim 400\,000$ births.² Globally, the World Health Organization reports that 15×10^6 preterm births occur every year and this number is increasing rapidly.³ Preterm birth complications have been recognized as the main cause of death for children aging less than 5 years, accounting for around 1×10^6 deaths in 2015.⁴ Additionally, the survival rate for preterm neonates that are 28 weeks or less gestational age is extremely low (less than 50%).⁵

Respiratory distress syndrome (RDS) or hyaline membrane disease has been recognized as the second major cause of mortality in neonates.⁶ In 2005, the number of cases with RDS

increased to 12.7% from 11.6% in 2003.⁷ Since lungs are among the last organs to fully develop, preterm and term neonates suffering from RDS require additional breathing support, such as mechanical ventilation, until their lungs are fully developed. However, the positive pressure applied during mechanical ventilation could cause morbidities, such as necrotizing bronchiolitis and alveolar septal injury with inflammation and scarring,^{8,9} resulting in some long-term complications such as bronchopulmonary dysplasia (BPD) and hypoxic ischemic encephalopathy (HIE).^{10,11} Extra-corporeal membrane oxygenation (ECMO) is the method of choice when mechanical ventilation is not sufficient and preterm neonates need external oxygenation support. However, ECMO is an invasive method and requires surgery to connect the device directly to the central blood vessels. Hollow fiber membrane based ECMO are used for this purpose to provide adequate gas exchange. Although the current oxygenators have shown promising life-saving results for treating respiratory failure in adults, they are not well suited for use with preterm and term neonates suffering from RDS due to their high priming volume and considerable pressure drop. Their high priming volumes requires that they will be filled with donor blood instead of saline, which can lead to complications. The high pressure drop necessitates an external pump for perfusion which can damage the blood cells.^{12,13} It should be noted that the total blood volume of a neonate is $95\text{--}100 \text{ ml kg}^{-1}$.⁸ Therefore, oxygenators should have a low priming volume ($\sim 10 \text{ ml kg}^{-1}$ of body weight) in order to use saline as a filling solution and to avoid excessive dilution of blood and consequent reduction in hematocrit.⁸ Such a device as well as the required extracorporeal circuit would have a priming volume which is compatible with clinical dosage of saline solution boluses of $10\text{--}20 \text{ ml kg}^{-1}$ for neonates with hypotension.^{14,15}

Consequently, a passive lung assist device (LAD), pumped by the baby's heart (the arterio venous pressure differential for a neonate is between 20 and 60 mmHg) and capable of gas exchange in ambient air, would be ideal; a concept termed as the artificial placenta. Such a LAD could be connected to the umbilical vessels to ameliorate the poor gas exchange capability of under-developed lungs during their final stages of growth and maturation. The recent development of microfluidic technology that enables fabricating high surface to volume ratio fluidic networks^{16,17} is especially suited for an artificial placenta device with low priming volume, low hydraulic resistance (low pressure drop), and high gas transfer in ambient air. Over the past decade, many microfluidic oxygenators have been developed, yet only a few of them^{9,18,19} could be perfused solely by the arterio venous pressure differential and work in ambient air without the need of external gas supply. Most of other microfluidic blood oxygenators were designed to be operated with the assistance of an external pump, which can cause complications such as hemolysis,^{20,21} or required additional actively perfused gas supply, such as pure oxygen or compressed air to enhance to gas exchange.^{16,17,22\text{--}30}

One limitation of the previous pumpless, ambient gas exchange oxygenators^{9,18,19} has been that only one side of the microfluidic network, through which the blood flows, is composed of the thin gas exchange membrane. This limitation can be overcome by incorporating thin gas exchange membrane on both sides albeit with additional fabrication complexity. Indeed, oxygenators with double-sided gas exchange microfluidic channels have been previously developed.^{29,31} They have a microfluidic oxygen supply and distribution manifolds on their either side which serve to stabilize the membrane and prevent their distortion, delamination, and failure under operating pressures. However, these manifolds require that the exchange gases be pumped through them and are not suited for the artificial placenta configuration where gas exchange with the ambient atmosphere is sought. In addition, exchange of gases with air at ambient pressure is preferable to 100% oxygen at high pressure due to complications such as hyperoxemia and oxygen toxicity.³² In this study, we report a new technique to fabricate a thin microfluidic blood oxygenator (SOU) that is capable of gas exchange from both the top and bottom sides of the blood channel network. Consequently, the gas exchange area of the device is increased to improve gas exchange capacity, while its overall priming volume was not changed. Blood testing was performed to measure the performance of SOUs under realistic clinical settings. This optimized configuration was used to build a LAD by connecting several SOUs together. Blood testing was performed to measure the performance of SOUs and the

LAD under realistic clinical settings. This new design, enabled by the new fabrication process, is the first pumpless artificial placenta device capable of achieving the required oxygen gas exchange to support neonates with RDS.

METHODS

Design

A new design (Fig. 1) of the single oxygenator unit (SOU) was developed, which consisted of two main components: (i) a blood vascular network that is responsible for facilitating blood flow distribution by forming a thin blood layer close to the membranes for gas exchange and (ii) two gas permeable membranes that form the top and the bottom of the vascular network to allow gas transfer. The channel layout for the blood vascular network was adapted from the previous designs that had been optimized for uniform distribution of the blood over a large surface and with no dead zones, low hydraulic resistance, and low shear stresses encountered by blood.¹⁸ This design [Figs. 1(a) and 1(b)] consisted of a square-shaped chamber filled with arrays of square-shaped micropillars that formed an interconnected blood flow network. The micropillars provided mechanical support to hold large area membranes apart and maintained the blood vascular network integrity during operation. Optimal pillar size of 1×1 mm was found to be most suitable¹⁹ for reliable bonding of the gas exchange membrane to the blood channel network and therefore was used here. The initial size of the blood vascular network was $43 \text{ mm} \times 43 \text{ mm}$ with three different depths of 75, 110, and $145 \mu\text{m}$ which produced pressure drops that spanned the range of arterio venous pressure differences in neonates. This layout allowed 76% of the gas exchange membrane area to be involved in gas transfer. Two pieces of silicone tubes (3.6 mm ID) were diagonally placed on two opposite corners to serve as an inlet and outlet.

The gas exchange membrane used consisted of a stainless-steel reinforced thin ($50-\mu\text{m}$) PDMS membrane on one side that was adapted from our previous work.¹⁹ The composite membrane consisted of an ultra-thin stainless-steel mesh (MS-400/19, Asada Mesh Co. Ltd.) with a thickness of $39 \pm 2 \mu\text{m}$, a pore size of $45 \mu\text{m}$, and a porosity of 49% which was covered with PDMS to form a $50 \mu\text{m}$ -thick membrane. Additionally, a new fabrication process was developed in this paper which facilitated the incorporation of a slightly thicker ($150-\mu\text{m}$) steel reinforced membrane on the other side of the blood channels as well, in order to facilitate higher gas exchange. The new fabrication process enabled a 100% increase in the surface area for gas exchange while maintaining the priming volume, pressure drop, and other hydraulic characteristics of the device and was incorporated to increase the oxygenation performance. The older design¹⁹ [Fig. 1(c)] consisting of thin gas exchange membrane on one side was also fabricated and tested for comparison purposes.

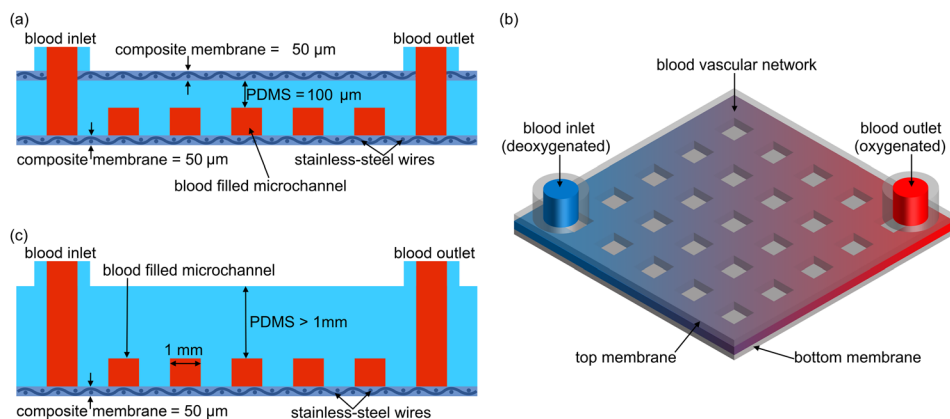


FIG. 1. (a) Schematic cross-sectional view of a SOU with double-sided gas diffusion membrane, (b) schematic 3D view of a double-sided SOU, and (c) schematic cross-sectional view of a SOU with single-sided gas diffusion membrane.

Fabrication

Previously, we had developed a microfluidic blood oxygenator with a new composite membrane and single-sided gas diffusion blood channels.¹⁹ One side of the oxygenator was composed of a stainless-steel mesh reinforced, thin PDMS membrane that was stiff and prevented any deformation under the operating pressure while still allowing efficient gas exchange. However, the other (top) side, which contained the microchannel network embedded in it, was composed of a thick (more than 1 mm) PDMS layer which was required in the fabrication process to attach to the thin PDMS membrane firmly and peel off without any deformation or defects. In order to improve the gas exchange characteristics, attempts were made to reduce the thickness of the top side to anywhere between 50 and 200 μm so that gas exchange can occur on both sides. However, these attempts proved unreliable and defects were generated while peeling off a large area ($\sim 20 \text{ cm}^2$) thin PDMS membrane layer with embedded microchannel network. In this paper, we have developed a new fabrication process where the stainless-steel mesh is incorporated into both sides of a thin cast part consisting of the microfluidic network. This fabrication process also ensures that the stainless-steel mesh is firmly embedded in the PDMS and is not exposed to the blood at any location. The incorporation of the stainless-steel mesh provides structural support to the thin (250–500 μm) but large microfluidic layer ($\sim 20 \text{ cm}^2$). This reliable fabrication process enables for the first time, high yield manufacture of the double-sided oxygenator units that can achieve high gas exchange and better performance.

Microfluidic blood oxygenators with double-sided gas diffusion were fabricated using a modified PDMS soft-lithography process as shown in Fig. 2. First, the negative template of the blood vascular network for both designs (single-sided and double-sided) was fabricated by patterning on SU-8 3035 (Microchem Corp, Westborough, MA, USA) using a conventional photolithography technique³³ [Fig. 2(a)]. PDMS (Sylgard 184, Dow Corning, Midland, MI) was prepared by mixing the base and the curing agent together in 10:1 ratio by weight. A desiccator was used for 30 min to degas the mixture. PDMS was spin-coated on the microchannel mold with the speed of 500 RPM for 60 s to form the vascular network as shown in Fig. 2(b). Subsequently, this spin coated layer was heated up to 85 °C in an oven to cure the PDMS while in the mold. A second layer of PDMS was spun with a speed of 4000 RPM for 40 s on top of the cured PDMS to form a 25- μm -thick PDMS layer. A piece of ultra-thin stainless-steel mesh was embedded into the wet PDMS as shown in Fig. 2(c). (To avoid exposing stainless-steel mesh to blood, two holes were cut into the mesh at the inlet and the outlet positions by a

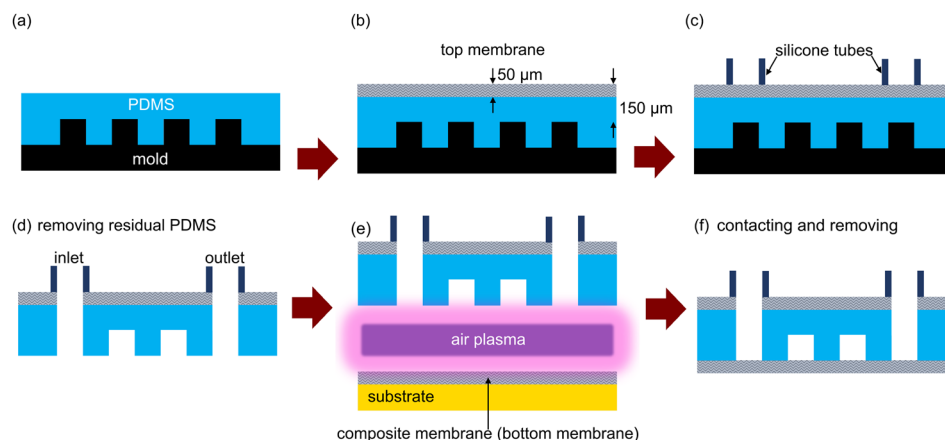


FIG. 2. Fabrication process of a dsSOU: (a) a thin layer of PDMS was spin-coated on the top of mold and the product was placed in an oven to cure PDMS, (c) another thin layer of PDMS was spin-coated on the top of the cured PDMS and a piece of stainless-steel mesh was embedded into wet PDMS, following a third spin-coated PDMS layer (d) silicone tubes were placed on two opposite corners as the inlet and outlet, (e) the device was peeled off and residual PDMS inside inlet and outlet was removed, and (f) the bottom surfaces of the vascular network and the composite membrane were exposed to air plasma, the blood vascular network and the membrane were brought in contact and placed in an oven at 85 °C overnight, and the substrate was removed.

scalpel and was carefully aligned and placed on top of the vascular network.) The composite reinforced microfluidic layer was placed in an oven at 85 °C for 10 min to cure the PDMS. Subsequently, a third layer of PDMS was spin-coated on top of the previous layer with the same speed and cured in an oven at 85 °C for 10 min as seen in Fig. 2(d). For the inlet and outlet, two 10-mm-silicone tubes (MasterFlex platinum-cured silicone tubing) were attached diagonally on two opposite corners of the vascular network using wet PDMS [Fig. 2(e)] and cured at 85 °C for an hour to strengthen gluing between tubes and the vascular network. The device was peeled off from the mold, and the residual PDMS inside tubes was removed by a biopsy punch [Fig. 2(f)]. This new approach of layer by layer fabrication of the microfluidic base layer enables highly reliable fabrication of pinhole free layer area thin microfluidic networks that are critical for the oxygenator.

The composite membrane was produced as previously described.¹⁹ In short, PDMS was spin-coated on a substrate at 4000 RPM for 40 s and a piece of ultra-thin stainless-steel mesh was laid on the uncured PDMS; then it was cured in an oven at 85 °C for 30 min. A second layer of PDMS was spin-coated on the cured product with the same speed and time and cured in an oven at 85 °C for 30 min. Once the vascular network and the membrane were ready, they were bonded to each other by using a hand held air plasma³⁴ (BD-20AC Laboratory Corona Treater, Electro-Technic Products, Chicago, IL, USA) as shown in Fig. 2(g). Their activated surfaces were brought in contact and formed a strong bonding with each other as shown in Fig. 2(h). The device was stored in an oven at 85 °C overnight to strengthen the bonding. Finally, the device was removed from the substrate and was ready to use [Fig. 2(i)]. Figures 3(a) and 3(b) show a dsSOU filled with bovine blood.

Smaller dsSOUs with three different heights of 75, 110, and 145 μm for the microfluidic blood vascular network were fabricated and tested to compare their performance with single sided oxygenators. All smaller double-sided devices had the same dimensions for the blood vascular network (43 mm \times 43 mm) with an effective gas exchange surface area of 14.08 cm^2 but with different priming volume of 0.106 (75 μm), 0.156 (110 μm), and 0.204 ml (145 μm), respectively.

The SEM image of the cross-section of a fabricated dsSOUs is shown in Fig. 3(c). The top and bottom membranes have a thickness of 50 and 150 μm , respectively. Therefore, both the top and bottom surfaces can participate effectively in gas exchange between the blood flowing in the channel and the ambient air surrounding the device. Also, it can be seen that the stainless-steel wires are completely embedded in the PDMS and will not be exposed to the blood flowing inside the channels. X-ray photoelectron spectroscopy (XPS) analysis of the surface of a PDMS and a composite membrane [Fig. 3(d)] showed that the elemental compositions at the surface of the PDMS coated stainless steel mesh was similar to PDMS and did not show any Fe which would indicate any exposed steel. Filling in this device is also uniform as shown in Figs. 3(e)–3(h) (multimedia view), and there are no dead zones created that could promote clot initiation.

Larger SOUs (91 mm \times 91 mm) with blood vascular network with a height of 200 and 245 μm and a priming volume of 1.25 and 1.53 ml was also fabricated, as shown in Fig. 3(i), in order to be incorporated in the LAD. The large SOUs have 4-fold larger gas exchange surface area (62.56 cm^2) and only four of them are required to support the gas exchange needs of a 1–2 kg neonate. The use of large SOUs significantly reduced the priming volume associated with the interconnects and the two interconnect designs (LAD 1 and 2), as shown in Fig. 4, had a total priming volume of only 17 and 8 ml of blood.

Requirements for an artificial placenta type oxygenator

In the artificial placenta type configuration, the lung assist device (LAD) is placed in parallel to the body's systemic circulation such that the inlet is connected to an artery and the outlet to the vein. This is to ensure that the arterio-venous pressure difference that pumps blood through the body will also perfuse the device. This kind of connection is in contrast to other commonly used ECMO devices that use external pumps which are usually connected to the

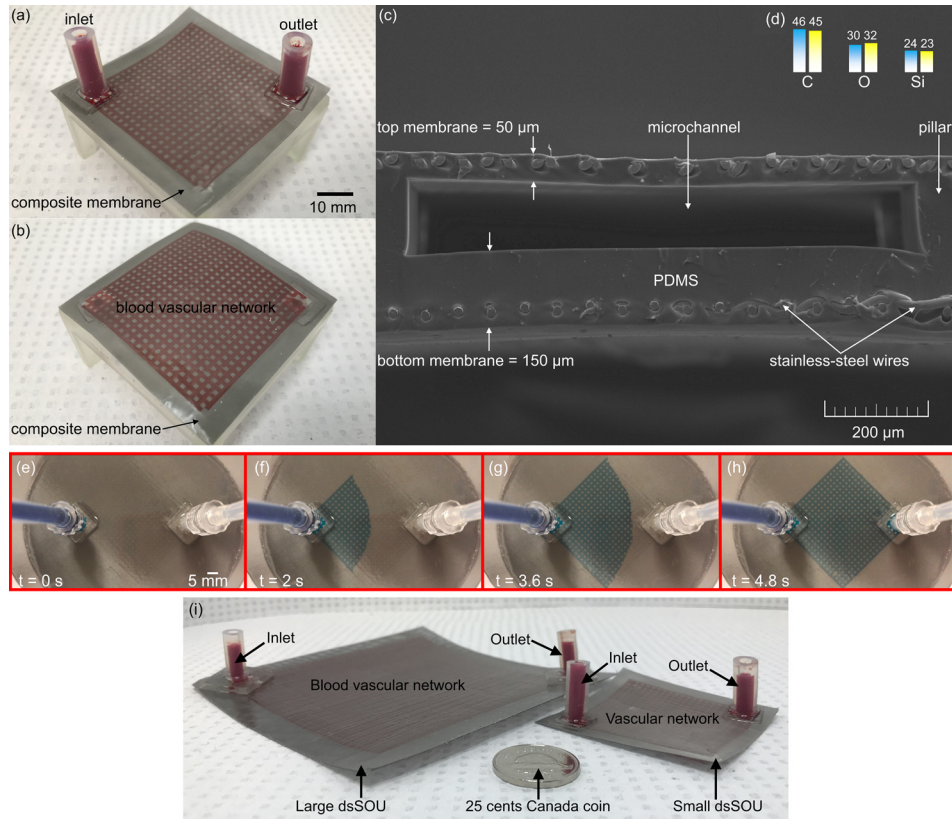


FIG. 3. (a) Image of the top-side of a double-sided SOU filled with bovine blood, (b) image of the back-side of the same SOU filled with bovine blood, (c) SEM image of a double-sided SOU, (d) the XPS analysis of both PDMS and composite membranes (blue bars represent for composite membrane and yellow ones represent for PDMS membrane), (e)–(h) sequence of filling a dsSOU with the height of $\sim 110 \mu\text{m}$ with dyed water (flow rate = 2 ml/min) and (i) image of a small dsSOU besides a large dsSOUs for size comparison (both devices were filled with bovine blood). The coin shown in the figure is a Canadian 25-cent piece (approx. 20 mm diameter). Multimedia views: <https://doi.org/10.1063/1.5034791.1>; <https://doi.org/10.1063/1.5034791.2>

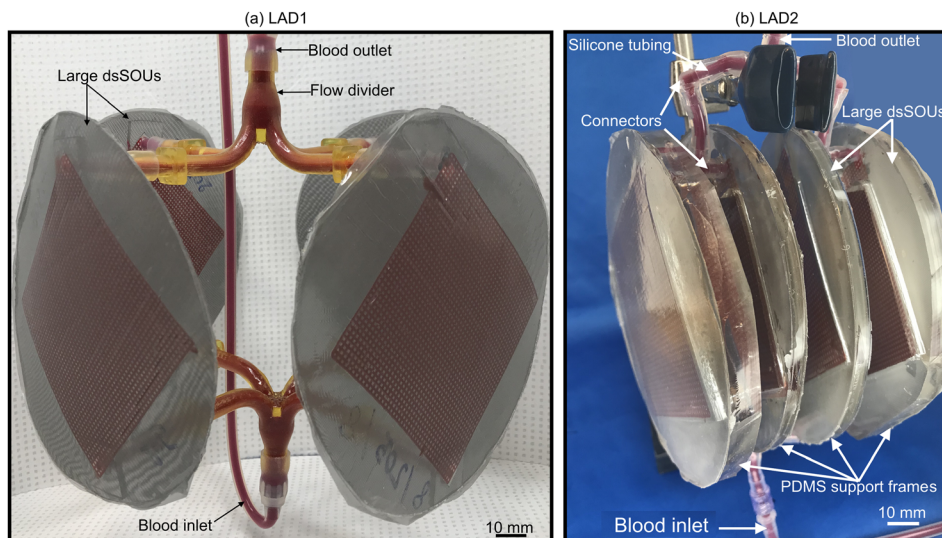


FIG. 4. (a) Image of the LAD1 with four large dsSOUs with a total priming volume of 17 ml and (b) image of the LAD2 with four large dsSOUs which were connected by connectors and silicone tubing with a total priming volume of 8 ml. Both LADs were filled with bovine blood.

body in venous-artery or venous-venous configuration.³⁵ The arterio-venous connection places specific constraints on the design of the devices. Blood which enters the LAD is arterial blood. As a result, the blood has already passed through the lungs where it has been oxygenated before it enters the LAD. Under lung failure and/or pulmonary hypertension, the arterial blood may only be 10%–30% below full saturation. Therefore, compared to current ECMO oxygenator, our LAD is designed to work at the upper end of the oxygen binding curve of haemoglobin.⁸ Further, the LAD should have a low dead volume (typically 10%–20% of the 100 ml/kg body weight) so that it could be filled with saline and not require blood transfusion. The LAD should also not induce high cardiac output failure due to excessive bypass blood flow from the systemic circulation. As a result, the LAD should operate under flow rates of 20 to 30 ml min⁻¹ kg⁻¹ of a baby. The oxygen saturation of the incoming blood is estimated at 70%.³⁶ Blood with an average haemoglobin concentration of 16 g dl⁻¹ and oxygen binding capacity of 1.39 ml oxygen per one gram of haemoglobin is considered in this calculation.^{37,38} At blood flow rates from 20 to 30 ml min⁻¹ kg⁻¹ of a baby, the LAD would need to deliver 1.3 to 1.9 ml of O₂ min⁻¹ kg⁻¹ of a baby. This is the maximum amount of oxygen which could be taken up by the blood with a blood flow of 20 to 30 ml min⁻¹ kg⁻¹ of a baby.^{8,9,18} Consequently, during testing, the oxygen saturation level in blood before the LAD was adjusted to 59 ± 3% (lower than the physiological values) so that it could be increased to 90% or higher to determine the maximum gas transfer capability of the LAD that is designed to support neonates weighing up to 2 kg.

Gas exchange testing in blood

In vitro gas exchange testing was performed on these oxygenators using blood to assess their performance. Before perfusing the device with blood, deionized water was used to prime the device so as to ensure a uniform blood flow and prevent trapping of air bubbles. Then, heparinized (3 units ml⁻¹) bovine blood (Bovine 7200807-1L, Lampire Biologicals Laboratories, Pipersville, PA) was used to evaluate oxygen transfer in the device. The oxygen concentration in blood was adjusted to venous conditions to mimic *in vivo* oxygenation provided by the natural lungs. In order to achieve a target saturation level, a hollow fiber oxygenator (PDMSXA-1.0, PermSelect®, Ann Arbor, MI, USA) was used. Blood was pumped through the shell of the hollow fiber membrane by a peristaltic pump (Ismatec model ISM832C, Ismatec, Glattbrugg, Switzerland) at 15–25 ml min⁻¹, while a carbon dioxide/nitrogen gas mixture (5%/95% v/v) was introduced through fibers at 201 h⁻¹ to reach a desired oxygen saturation level of 63% ± 5%. Then, blood was stored in a sealed bottle and placed in a fridge at 4 °C overnight to minimize the oxygen metabolism by cells and maintain the set oxygen saturation level. The next day, blood was transferred to 140-ml syringe (Monoject™) and a cap was used to tightly close the syringe for further use. Before transferring blood to syringes, a stir bar was placed inside of each syringe.

A 140-ml syringe filled with heparinized blood was loaded to a syringe pump (22 syringe pump, Harvard Apparatus, Holliston, MA, USA) and magnetic stirrer was located under the syringe (Fig. 5). The stir bar inside the syringe provided sufficient mixing in blood to keep it homogeneous throughout the experiment. The blood was perfused through the microfluidic oxygenator. The flow rate was varied from 0.5 ml min⁻¹ to 4 ml min⁻¹ for dsSOUs and ssSOU.

A TruWave Pressure Transducer (Edwards Lifesciences LLC, Irvine, CA, USA) was placed before the device and connected to a Spacelabs 90369 Patient Monitor (SpaceLabs Medical, Inc., Redmond, WA, USA) to monitor the pressure drop during the experiment. Blood was analyzed by a point-of-care blood gas analyzer (GEM Premier 3000, Instrumentation Laboratory, Lexington, MA, USA) before and after the device to assess the oxygen content in blood and determine the rate of oxygen uptake by the device. Also, the hematocrit content was measured by a Complete MicroHematocrit System (StatSpin CritSpin, Norwood, MA, USA). The total concentration of oxygen in the blood was calculated by taking the sum of the amount of dissolved oxygen and the hemoglobin-bound oxygen.¹⁸

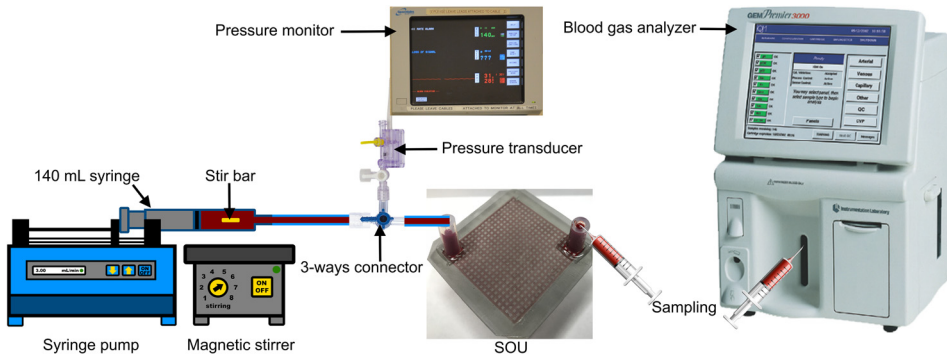


FIG. 5. Experimental setup for gas exchange testing in blood.

To evaluate the maximum oxygen transfer capacity of oxygenators, an enriched oxygen environment was created around oxygenators by placing them inside an airtight chamber (200 mm × 300 mm × 120 mm) made of acrylic. Once the oxygenator was placed inside of the chamber, it was filled with pure oxygen so that it completely fills the chamber and sealed at atmospheric pressure.

RESULTS AND DISCUSSION

Comparison between the performance of single and double sided single oxygenator units

dsSOUs with three heights of 75, 110, and 145 μm were fabricated and tested with blood to select the appropriate height that could produce pressure drop in the operational regime (20–60 mmHg). The devices were tested at various blood flow rates of 0.5, 1, 1.5, 2, 3, and 4 ml min^{-1} (Fig. 6). For all tested devices, pressure drop linearly increased with blood flow rates as shown in Fig. 5. Also, it was observed that the pressure drops decreased with increasing channel height from 75 μm to 145 μm as expected. The gray region in Fig. 6 shows the operation regime for successful pumpless operation of the artificial placenta device. It can be seen that devices with a channel height of 75 μm was not suitable as the pressure drop is higher than the operational regime. However, both devices with channel height of 110 and 145 μm had lower pressure drops than 60 mmHg over a significant range of blood flow rates and could be considered for this application. As a result, dsSOUs with the channel height of 110 μm was chosen as the optimum device for further experiments.

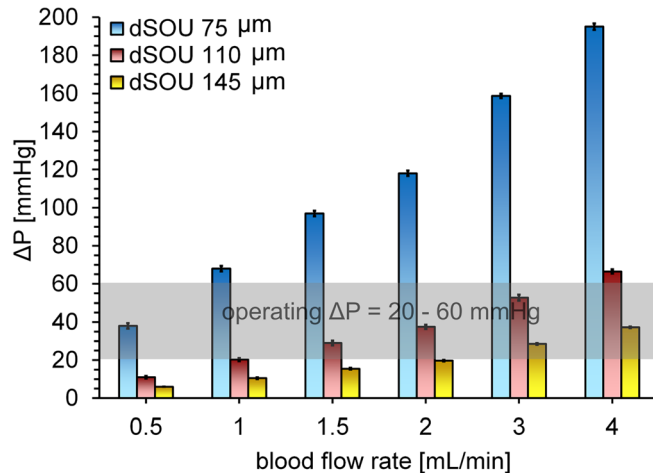


FIG. 6. Pressure drop of dsSOUs at various blood flow rate for different heights. Data are mean \pm SD, n = 4.

Then, both ssSOUs and dsSOUs (with channel height of $110\text{ }\mu\text{m}$) were fabricated and their gas exchange performance measured in order to characterize the improved performance. *In vitro* gas exchange testing was conducted flowing blood at various flow rates of 0.5, 1, 1.5, 2, 3, and 4 mL min^{-1} while simultaneously measuring the increase in partial pressure of oxygen (pO_2) and oxygen saturation level (SaO_2) between the inlet and outlet of the oxygenator. The experiment for each type of devices was repeated 4 times and the average was calculated for each condition. Each device was first tested in ambient air and then in an enriched oxygen environment. The results shown in Fig. 7 demonstrate that the oxygenation of blood is always better when dsSOUs are used as compared to ssSOUs.

Simultaneously, the pressure drops of both ssSOU and dsSOUs were measured with flow of blood and no significant difference was observed as shown in Fig. 7(a). This result confirmed that the dsSOU, despite being thin, is stiff and does not undergo any structural change under the operating pressure that could affect its performance. It also confirmed that the differences in performances observed was solely due to the higher gas transfer area enabled by exposure of the blood to oxygen from both sides and not due to any other factors.

Gas exchange tests showed that the ssSOU increased the oxygen saturation of the blood. This effect decreased gradually with the increase in blood flow rate, as shown in Fig. 7(b) when exposed to air at atmospheric pressure. Exposure to pure oxygen environment at atmospheric pressure allowed the increase in oxygen saturation to be stable till flow rates were less than 3 mL min^{-1} before falling at higher flow rates, as shown in Fig. 7(c). Additionally, the experimental results for ssSOUs showed that increasing blood flow rate, especially at lower blood flow rates ($0.5\text{--}1.5\text{ mL min}^{-1}$), resulted in a gradual increase in the oxygen uptake [Fig. 7(d)]. However, at higher blood flow rates ($1.5\text{--}3\text{ mL min}^{-1}$), the oxygen uptake remains constant and even decreased at a blood flow rates $> 3\text{ mL min}^{-1}$. This behaviour could be a result of the competing effects of increased volume of blood flowing in the device and the reduced residence time of each of the red blood cells in it. Alternatively, at higher flow rates, the membranes are flexed which could increase the effective channel height and a lower oxygen uptake.

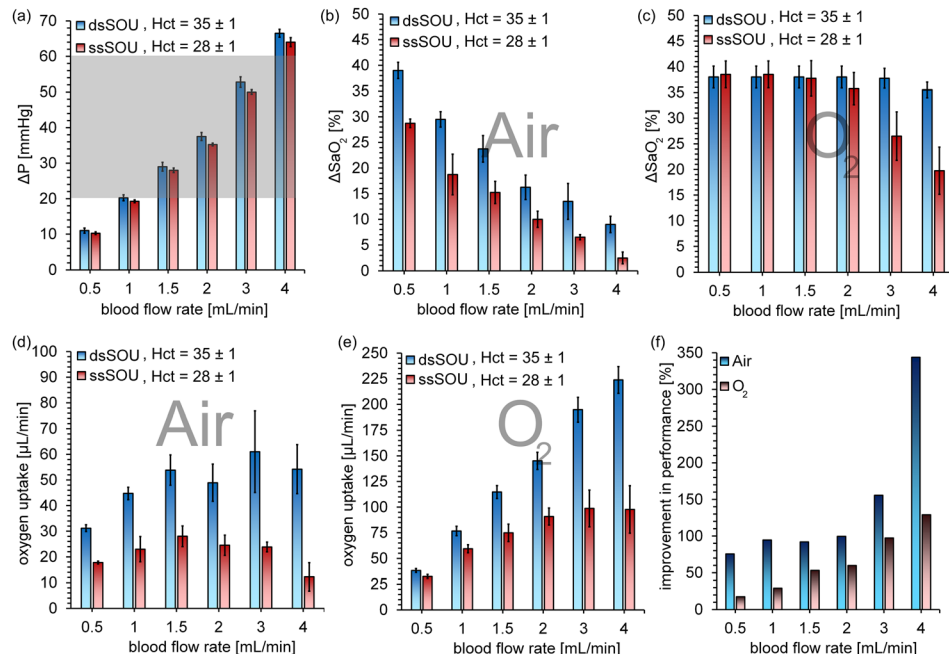


FIG. 7. *In vitro* comparison between ssSOUs and dsSOUs: (a) pressure drop, (b) the increase in oxygen saturation level in room air, (c) the increase in oxygen saturation level in an enriched oxygen environment with atmospheric pressure, (d) the oxygen uptake for room air, (e) the oxygen uptake in an enriched oxygen environment with atmospheric pressure, and (f) the improvement in performance for dsSOUs compared to ssSOUs. Hematocrit (Hct) level is shown for both ssSOUs and dsSOUs. Data are means \pm SD, $n = 4$.

At high flow rates, only the layers close to the gas exchange membrane have sufficient flux of oxygen molecules to attain saturation and a significant amount of blood away from the membrane remained unsaturated as it leaves the device. The results also show that the oxygen uptake of ssSOUs was enhanced in an enriched oxygen environment [Fig. 7(e)]. The oxygen uptake increased steadily with flow rate until 3 ml/min and then stabilizes. No further reduction in oxygen uptake was observed at higher flow rate. This behaviour can be attributed to the higher oxygen flux through the membrane due to the higher concentration gradient across it under enriched conditions.

The dsSOUs were found to perform better than the ssSOUs under all flow conditions as shown in Fig. 7. The change in oxygen saturation (ΔSaO_2) also decreased for dsSOUs when the flow rate was increased which was similar to the ssSOUs. However, the rate of the decrease was smaller compared to ssSOUs in room air [Fig. 7(b)]. Interestingly, in pure oxygen environment, the blood was fully saturated at flow rates below 3 ml min^{-1} and consequently the ΔSaO_2 was found to remain constant at these flow rates [Fig. 7(c)] and decrease at higher flow rates. It should be noted that the superior performance of dsSOUs was also under conditions when the hematocrit (Hct) of the blood used for testing is higher as compared to ssSOU. Blood with lower hematocrit value can be saturated with lesser amount of oxygen and if both were tested with blood with same Hct values, the difference in performance will be even larger.

Consequently, the oxygen uptake for dsSOUs was found to be significantly higher compared to ssSOUs, especially at higher blood flow rates [Fig. 7(d)]. For instance, at a blood flow rate of 4 ml min^{-1} , the dsSOU produced an oxygen uptake of 54.2 $\mu\text{l min}^{-1}$, while it was only 12.2 $\mu\text{l min}^{-1}$ for the ssSOU operating under the same conditions. This represents a 343% [Fig. 7(f)] improvement in oxygenation due to exposure of both sides of blood vascular network to ambient air. The oxygen uptake of dsSOUs was also found to increase with the increase in blood flow rate and stabilize at higher flow rates [Fig. 7(d)]. Unlike the ssSOU exposed to ambient air, no drop in oxygen uptake was observed at the highest tested flow rate of 4 ml min^{-1} . The access to oxygen from both sides of the blood vascular network in dsSOUs reduces the effective diffusion length for the oxygen to travel by half thereby providing a more stable oxygen uptake at higher flow rates. Like ssSOUs, dsSOUs were also tested in an enriched oxygen environment [Fig. 7(e)]. The oxygen uptake was found to continuously increase with increasing blood flow rate. It was also found to be higher as compared with ssSOUs. For instance, the oxygen uptake at a blood flow rate of 4 ml min^{-1} was 223.8 $\mu\text{l min}^{-1}$ for dsSOUs which shows 129% [Fig. 7(f)] improvement in oxygen uptake over the ssSOU under similar conditions. This behaviour can also be attributed to the higher concentration gradient across the membrane that produces a high flux of oxygen which is able to sustain the continued increase in oxygen uptake.

Finally, dsSOUs with different heights were tested with bovine blood to evaluate their performance under the same conditions (Fig. 8). As seen in Fig. 8(a), oxygen uptake of dsSOUs with different heights was not significantly different, especially at higher blood flow rates. This could be because of lower resistance time for blood in microchannels which limits the gas exchange to the regions close to both membranes. Although the oxygen uptake was improved by exposing oxygenators to pure oxygen, they still had the same behaviour [Fig. 8(b)]. These results reveal that decreasing the height of blood channel would increase gas exchange but not significantly. Therefore, pressure drop and its suitability for pumpless operation would be the key factor in determining the suitable height of the oxygenator for artificial placenta application.

Scaling of double-sided SOUs

Very few microfluidic oxygenators have been shown to be capable sustaining a large blood flow ($\sim 10 \text{ ml/min}$) at reasonable pressure drop (20–60 mmHg) and oxygenating blood sufficiently. This is primarily due to the small size of the microchannels (which causes high resistance to blood and increasing pressure drop) and the inability to fabricate large area devices (which limits the residence time for sufficient oxygenation). Instead of stacking multiple smaller

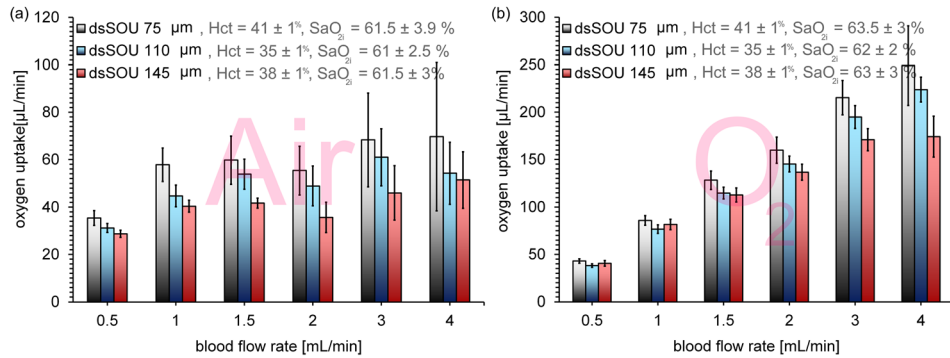


FIG. 8. *In vitro* gas exchange testing in blood for dsSOU with three different heights at various blood flow rates: (a) tested in room air and (b) tested in an enriched oxygen environment with atmospheric pressure. Oxygen saturation level at the inlet (SaO_{2i}). Data are mean \pm SD, $n = 4$.

SOUs, larger SOUs can be used as they would reduce the number of interconnections between the devices when the LAD is assembled and serve to reduce the overall priming volume of the oxygenator. For instance, by increasing size of the SOU to 91 mm \times 91 mm, the gas exchange surface area will have the same total gas exchange surface area as 4 smaller devices with the size of 43 mm \times 43 mm. This larger configuration will eliminate several interconnections needed and reduce the overall priming volume of the LAD.

Therefore, larger dsSOUs (91 mm in length) were fabricated with 200 and 245 μm in height to optimize to produce a pressure drop lower than 60 mmHg under the operating blood flow rates and were tested with blood over a wider range of blood flow rates from 1 ml min^{-1} to 12 ml min^{-1} in ambient air and under pure oxygen environment. The pressure drop of both large dsSOUs was found to linearly increase with blood flow rates as shown in Fig. 9. As seen in Fig. 9, there was no significant difference in the pressure drop of the two dsSOUs of different heights at various flow rates. It remains between 20 and 35 mmHg for flow rates between 8 and 12 ml/min . These results indicate that gas exchange characteristics should determine the optimal height of the device. The larger SOUs allow a much longer residence time of blood in the device as compared to the smaller SOUs although they operate at nearly the same pressure drop.

Subsequently, gas exchange experiments were performed on large dsSOUs with a height of 200 and 245 μm . The oxygen uptake of the blood perfused through the dsSOUs was found to gradually increase with increasing blood flow rates up to 7.5 ml min^{-1} and 12 ml min^{-1} in ambient air as shown in Figs. 10(a) and 10(c). Similar to the smaller dsSOUs, a better oxygen uptake was also achieved when exposed to pure oxygen in the ambient instead of room air for

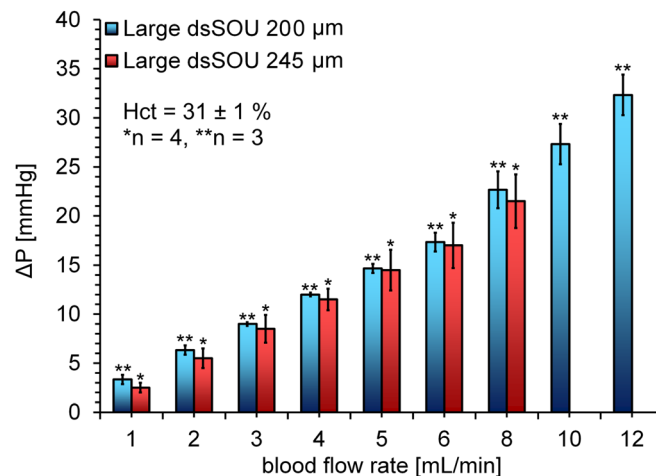


FIG. 9. Pressure drops of large dsSOUs tested with bovine blood at various blood flow rates. Data represents the mean \pm SD.

the large dsSOUs. The oxygen uptake at a blood flow rate of 8 ml min^{-1} was 0.44 and 0.52 ml min^{-1} for large dsSOUs with the height of 245 and $200 \mu\text{m}$, respectively, while the corresponding pressure drops were 21.5 and 22.7 mmHg . The higher flow rate, lower pressure drop, and the higher oxygen uptake obtained make the large dsSOUs suitable for integration into an LAD. In addition, the CO_2 release [Figs. 10(b) and 10(d)] was also measured.

The CO_2 release was not significantly impacted by changing ambient atmosphere from air to pure oxygen. For example, large dsSOUs with the height of $245 \mu\text{m}$ could release CO_2 at a rate of 0.27 ml min^{-1} and 0.26 ml min^{-1} in room air and pure oxygen environment, respectively. However, the height of the channels had a significant impact on the CO_2 release. For instance, at a blood flow rate of 8 ml min^{-1} and in a pure oxygen environment, the amount of CO_2 release was 0.26 ml min^{-1} in for dsSOU with a height of $245 \mu\text{m}$ as compared to 0.66 ml min^{-1} for dsSOU with a height of $200 \mu\text{m}$. Due to its superior performance in both oxygen and CO_2 exchange, large dsSOU with the height of $200 \mu\text{m}$ was chosen as the optimum configuration for using in LAD development.

It should be noted that a single large dsSOU could achieve an oxygen uptake as high as 0.59 ml min^{-1} at a blood flow rate of 12 ml min^{-1} and with a pressure drop of 32 mmHg when exposed to pure oxygen environment, which corresponds to a volume % transfer of 4.9% . In comparison, the small dsSOUs achieved an oxygen uptake of 0.17 ml min^{-1} at a blood flow rate of 3 ml min^{-1} with the same pressure drop. If four smaller dsSOUs were connected in parallel, an oxygen uptake of 0.68 ml min^{-1} can be achieved at a blood flow rate of 12 ml min^{-1} which is 14% more compared to the oxygen uptake of a single large dsSOU. The slightly poorer performance of the single large dsSOU can be attributed to the increased height of the fluidic channels which was required to ensure that the pressure drop was in the optimal range ($\sim 30 \text{ mmHg}$). Nevertheless, the combination of four smaller SOUs will have a significantly higher priming volume due to interconnections. Therefore, the larger dsSOUs, which had lower priming volume compared to a stack of smaller of SOUs, were used in the construction of the LAD and in subsequent testing.

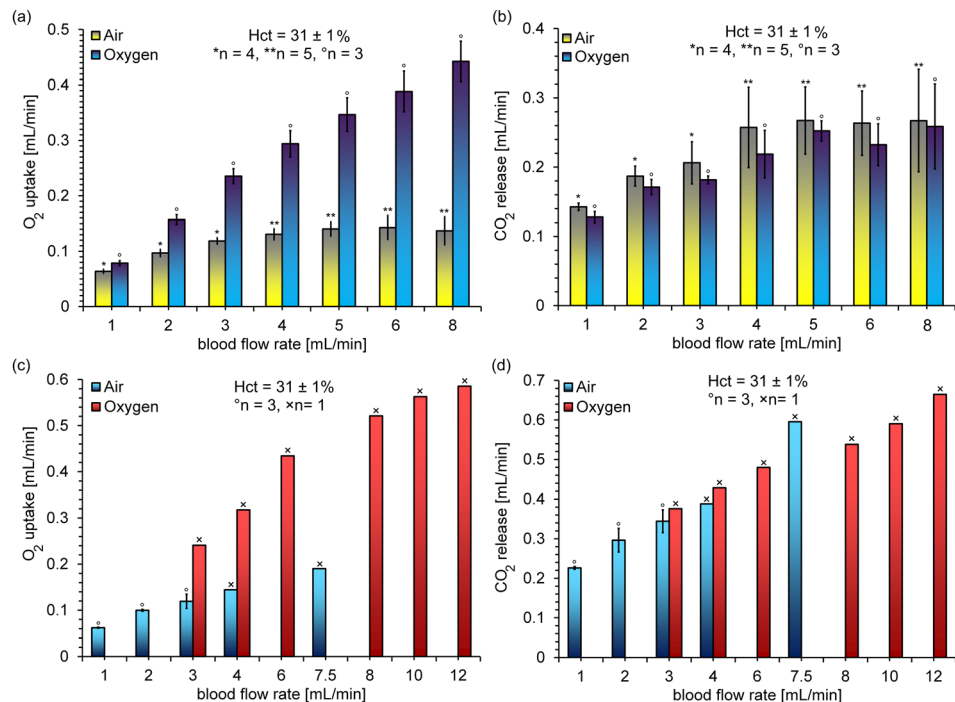


FIG. 10. *In vitro* performance of large dsSOUs: (a) oxygen uptake and (b) CO_2 release for devices with a height of $245 \mu\text{m}$, (c) oxygen uptake and (d) CO_2 release for devices with a height of $200 \mu\text{m}$ at various blood flow rates. Data represents the mean \pm SD.

Development of a compact LAD

The LAD was constructed by assembling 4 larger dsSOUs in parallel to meet the design requirements and to satisfy the estimated oxygenation needs of a neonate weighing up to 2 kg. A parallel design enabled a modular increase in the amount of flow that could be handled without changing the pressure drop or the oxygenation characteristics of the SOUs. Blood flow dividers were designed with symmetrical flow paths to connect the inlets of all the large dsSOUs to a central line (LAD1). In addition, the LAD was also reorganized into a different configuration by replacing flow dividers with connectors and silicone tubing (LAD2). First, the pressure drop of both LADs was measured with bovine blood with the same haematocrit level of $31 \pm 1\%$ to ensure both were operating in the same pressure drop range. Finally, the LAD1 was tested with bovine blood at blood flow rates of $10\text{--}60\text{ ml min}^{-1}$ in an enriched oxygen environment. Then, blood properties at the inlet and the outlet of the LAD were measured to determine the gas transfer capacity of the LAD.

The pressure drop of the LADs were measured at various blood flow rates from 10 to 60 ml min^{-1} as shown in Fig. 11(a). The pressure drop linearly increased with the blood flow rate and stayed within the optimum operating range [20–60 mmHg, the grey box shown in Fig. 11(a)] for all tested blood flow rates. The measured pressure drop of the LADs was the sum of pressure drops in large dsSOUs, flow dividers, connector, and tubing. To estimate the pressure drop contribution of the flow dividers, connector, tubing, and large dsSOUs, we calculated the difference between the LAD (flow of 10 ml min^{-1} through each large dsSOU; 33 mmHg for LAD1 and 38 mmHg for the LAD2) and a single larger dsSOU (flow of 10 ml min^{-1} , 27.3 mmHg), resulting as 5.7 mmHg and 10.7 or 17% and 28% of the total pressure drop, respectively. This showed the significant impact of flow dividers and connector tubing in the total pressure drop which would have been significantly higher if smaller double-sided SOUs were used.

The gas transfer of the LAD was measured when it was exposed to pure oxygen at atmospheric pressure. Figure 11(b) shows the oxygen saturation level in blood achieved at the outlet

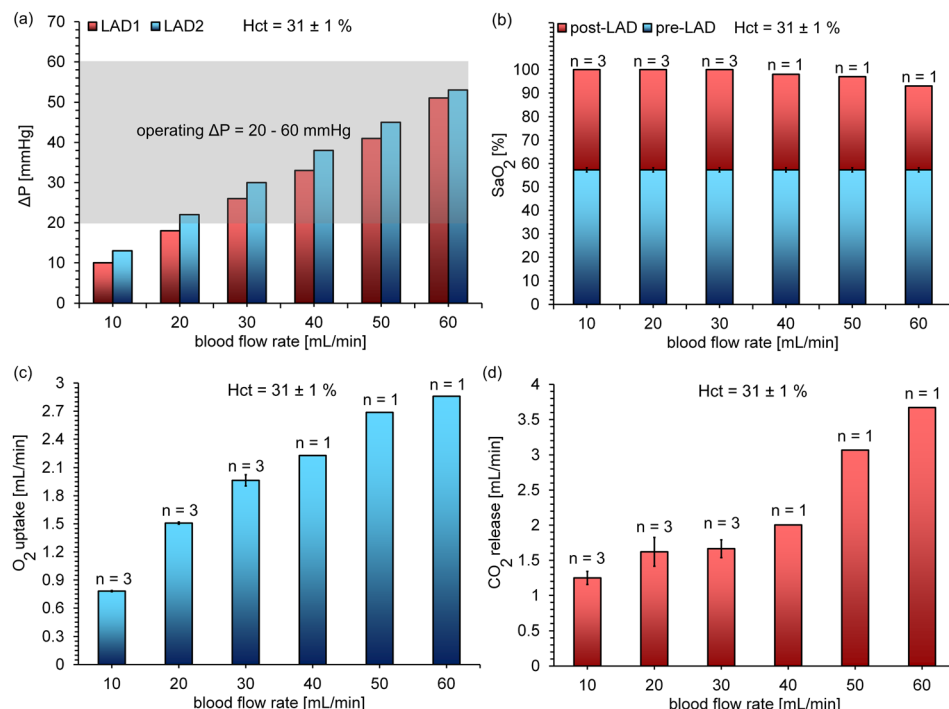


FIG. 11. *In vitro* test of the LADs with bovine blood at various blood flow rates: (a) pressure drop comparison between LAD1 and LAD2, (b) oxygen saturation level before and after the LAD1, (c) oxygen uptake for the LAD1, and (d) CO₂ release for the LAD1. Data are means \pm SD.

of devices by operating at various flow rates. The results showed that the blood exiting the LAD was fully oxygenated (100% saturation) for blood flow rates up to 30 ml min^{-1} which indicates that the LAD provided sufficient residence time and oxygen flux to completely saturate the incoming unsaturated blood (at $57 \pm 1\%$ saturation). However, beyond 30 ml min^{-1} flow rate, the oxygen saturation level at the outlet decreased but never dropped below 90% saturation. This behaviour was expected as the residence time of blood in the oxygenator reduced at higher flow rates. Nevertheless, the oxygen uptake continued to increase with flow rate even up to 60 ml min^{-1} as the larger volume of blood flowing through the oxygenator assists in carrying larger amount of oxygen. For instance, the oxygen uptake at blood flow rates of 30 and 60 ml min^{-1} was 1.96 and 2.85 ml min^{-1} [Fig. 11(c)]. Moreover, the CO_2 transfer was calculated and shown in Fig. 11(d) which showed a steady increase in CO_2 release over blood flow rates. This was expected as the thickness of boundary layer adjacent to membranes was reduced at higher blood flow rates resulting in better CO_2 exchange. In addition, as the same large dsSOUs were used to build the LAD2, it would be expected to see the same gas exchange properties without repeating the blood testing. These results demonstrate that this design of the LAD can provide the desired amount of oxygen delivery under proposed flow rates for preterm and term neonates with RDS.

The performance of the same LAD configuration when exposed to ambient air was also calculated using the experimental results obtained earlier for the larger double-sided SOUs and plotted. The LAD could achieve an estimated $\sim 20\%$ increase in oxygen saturation level (equal to an oxygen uptake of 0.8 ml min^{-1}) at a typical blood flow rate of 30 ml min^{-1} and a pressure drop of 26 mmHg for LAD1 or 30 mmHg for LAD2 in ambient air. In summary, compared to the previous LAD¹⁹ design developed for the artificial placenta, the new LAD with larger double-sided SOUs could achieve higher increase in oxygen saturation of blood, using lesser number of SOUs (and consequently lower priming volume) and at lower pressure drop.

Comparison to other microfluidic blood oxygenators

In summary, the performance of dsSOUs was found to be superior to the ssSOU design. In order to compare its performance with other microfluidic blood oxygenators,^{9,16–19,22,23,25–30} the reported oxygen transfer rate and blood flow rate could be normalized to the gas exchange surface area. So, the amount of oxygen uptake per 1 l of blood was calculated and defined as “oxygen transfer” to show the capacity of each device. This term also represents the amount of normalized oxygen transfer rate at a normalized blood flow rate of $11 \text{ min}^{-1} \text{ m}^{-2}$, which can be used for comparison purposes. Among all microfluidic blood oxygenators,^{9,10,16–19,22–30} the device developed by Rieper *et al.*²⁹ has the highest oxygen transfer of 60 ml of O_2 per liter of blood using oxygen as the perfusion gas. In comparison, the newly developed dsSOUs with a height of $75 \mu\text{m}$ exposed to a pure oxygen environment (without any gas pumping) achieved a higher oxygen transfer of 62.3 ml of O_2 per liter of blood. Even the dsSOUs with a height of $110 \mu\text{m}$ could achieve an oxygen transfer of 56 ml of O_2 per liter of blood in a pure oxygen environment which is comparable to the device made by Rieper *et al.*²⁹ It should be noted that this performance was also achieved at a lower pressure drop of 66 mmHg compared to the device made by Rieper *et al.*²⁹ with a pressure drop of 80 mmHg.

For the ideal pumpless implementation of the artificial placenta, the design criteria will be (i) an operating pressure drop of 20–60 mmHg, (ii) a minimum oxygen transfer of $1.3 \text{ ml of } \text{O}_2 \text{ min}^{-1} \text{ kg}^{-1}$ body weight, and (iii) a blood flow rate of $30 \text{ ml min}^{-1} \text{ kg}^{-1}$ of a body weight. This corresponds to an oxygen transfer of $43 \text{ ml of } \text{O}_2 \text{ l}^{-1}$ of blood kg^{-1} body weight to provide the required oxygen transfer for a baby. Figure 12 shows both pressure drop and priming volume versus the corresponding oxygen transfer for all microfluidic devices. Only those devices which are within the blue boxes fulfil the above stated criteria and have therefore the capability to be used as a pumpless oxygenator with low priming volume for the artificial placenta application using either oxygen or ambient air. To best of our knowledge, the LAD described in this paper, which was operated in a pure oxygen environment, is so far the only microfluidic-based oxygenator that meets all the requirements for an artificial placenta as indicated by the blue boxes.

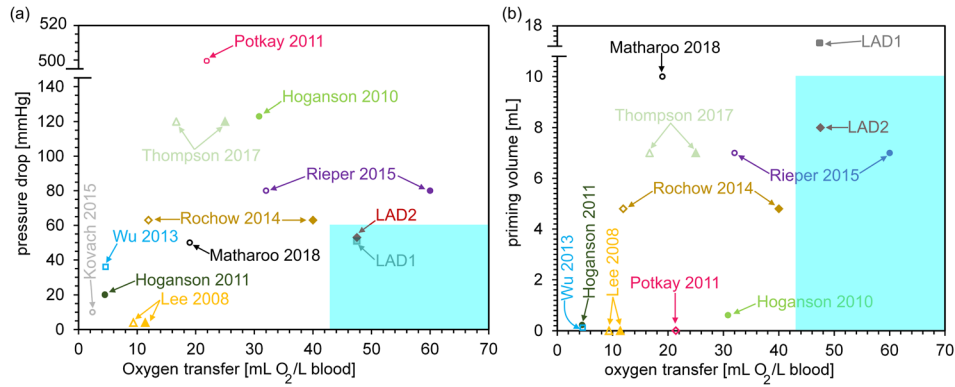


FIG. 12. Comparison of various oxygenators based on their oxygen transfer versus: (a) pressure drop and (b) priming volume (all data are extracted directly from each paper or calculated based on data reported). The same color and shape are used to show data from the same work. Only works that reported priming volume and pressure drop are included in these graphs. Open and filled shapes represent oxygen transfer in ambient air and enriched oxygen environment, respectively. The blue boxes show required oxygen transfer for an artificial placenta without the need of an external pump and a priming volume less than 10 ml. Single oxygenator units have low priming volume and are clustered on the x-axis.

Ongoing efforts are underway to increase the number of SOUs in the LAD to achieve a similar level of oxygen transfer in ambient air environment.

CONCLUSION

In this study, a new microfabrication technique for microfluidic blood oxygenators was established with double-sided gas transfer in blood channels, thereby improving gas exchange. Different heights of the blood vascular network were tested with bovine blood and the best one was compared to the device with single-sided gas transfer channels. Oxygen uptake of the double-sided device was increased up to 343% compared to the single-sided device. The dsSOUs would be ideal to fabricate a LAD which could fulfill all design criteria of an artificial placenta including required gas exchange, low priming volume, and capable of being operated by a baby's heart due to low pressure drop. Further, the size of dsSOUs was increased to be able to support higher blood flow rates with minimizing the priming volume of blood by using less connectors and tubing. Gas exchange properties of the large dsSOUs were not compromised significantly compared to the smaller dsSOUs. Subsequently, four large dsSOUs were fabricated and used to build a lung assist device (LAD) as an artificial placenta for preterm and term neonates suffering from RDS. The LADs consisted of 4 large dsSOUs with a low priming volume of 8 and 17 ml could provide enough oxygen to blood ranging from 1.96 ml min^{-1} to 2.86 ml min^{-1} using pure oxygen as ventilation gas. This LAD fulfills all design criteria of an artificial placenta including required gas exchange, low priming volume, and capable of being operated by a baby's heart due to low pressure drop. In the future, the design of the blood vascular network can be modified in a way to reduce hydraulic resistance in regions which have less contribution in gas transfer to achieve the same oxygen uptake at lower pressure drop. Additionally, antithrombin-heparin (ATH)^{39,40} or polyethylene glycol (PEG)⁴¹ can be coated on the surface of dsSOUs to improve anticoagulation properties of PDMS surfaces in which are contact with blood. Finally, newer designs that have higher gas exchange can be used to provide the sufficient oxygenation in ambient air.

ACKNOWLEDGMENTS

This work was supported by the Natural Sciences and Engineering Research Council of Canada (NSERC) and Canadian Institutes for Health Research (CIHR) through the Collaborative Health Research Program. P.R.S. also acknowledges the support from the Canada Research Chairs Program as well as the Discovery Accelerator Supplement grant.

- ¹J. A. Martin, B. E. Hamilton, M. J. K. Osterman, S. C. Curtin, and T. J. Mathews, *Natl. Vital Stat. Rep.* **66**, 1 (2017).
- ²B. E. Hamilton, J. A. Martin, and M. J. K. S. Osterman, *Natl. Vital Stat. Rep.* **65**, 1 (2015).
- ³World Health Organization, preterm birth fact sheet (2017).
- ⁴L. Liu, S. Oza, D. Hogan, Y. Chu, J. Perin, J. Zhu, J. E. Lawn, S. Cousens, C. Mathers, and R. E. Black, *Lancet* **388**, 3027 (2016).
- ⁵B. Bryner, B. Gray, E. Perkins, R. Davis, H. Hoffman, J. Barks, G. Owens, M. Bocks, A. Rojas-Peña, R. Hirschl, R. Bartlett, and G. Mychaliska, *J. Pediatr. Surg.* **50**, 44 (2015).
- ⁶R. Ramanathan, J. J. Bhatia, K. Sekar, and F. R. Ernst, *J. Perinatol.* **33**, 119 (2013).
- ⁷D. E. Schraufnagel, "Respiratory distress syndrome of the newborn," in *Breathing in America: Diseases, Progress, and Hope* (American Thoracic Society, New York, 2010).
- ⁸N. Rochow, E. C. Chan, W.-I. Wu, P. R. Selvaganapathy, G. Fusch, L. Berry, J. Brash, A. K. Chan, and C. Fusch, *Int. J. Artif. Organs* **36**, 377 (2013).
- ⁹N. Rochow, A. Manan, W.-I. Wu, G. Fusch, S. Monkman, J. Leung, E. Chan, D. Nagpal, D. Predescu, J. Brash, P. R. Selvaganapathy, and C. Fusch, *Artif. Organs* **38**, 856 (2014).
- ¹⁰R. J. Rodriguez, *Respir. Care* **48**, 279 (2003).
- ¹¹K. Fletcher, R. Chapman, and S. Keene, *Semin. Perinatol.* **42**, 68 (2018).
- ¹²A. Polito, C. S. Barrett, D. Wypij, P. T. Rycus, R. Netto, P. E. Cogo, and R. R. Thiagarajan, *Intensive Care Med.* **39**, 1594 (2013).
- ¹³R. de Vroege, M. Wagemakers, H. te Velthuis, E. Bulder, R. Paulus, R. Huybrechts, W. Wildevuur, L. Eijisman, W. van Oeveren, and C. Wildevuur, *ASAIO J.* **47**, 37 (2001).
- ¹⁴J. E. Palmer, *Vet. Clin. North Am. - Equine Pract.* **20**, 63 (2004).
- ¹⁵J. Brierley, J. A. Carcillo, K. Choong, T. Cornell, A. Decaen, A. Deymann, A. Doctor, A. Davis, J. Duff, M. A. Dugas, A. Duncan, B. Evans, J. Feldman, K. Felmet, G. Fisher, L. Frankel, H. Jeffries, B. Greenwald, J. Gutierrez, M. Hall, Y. Y. Han, J. Hanson, J. Hazelzet, L. Hernan, J. Kiff, N. Kissoon, A. Kon, J. Irazusta, J. Lin, A. Lorts, M. Mariscalco, R. Mehta, S. Nadel, T. Nguyen, C. Nicholson, M. Peters, R. Okhuyzen-Cawley, T. Poulton, M. Relves, A. Rodriguez, R. Rozenfeld, E. Schnitzler, T. Shanley, S. Skache, P. Skippen, A. Torres, B. Von Dessauer, J. Weingarten, T. Yeh, A. Zaritsky, B. Stojadinovic, J. Zimmerman, and A. Zuckerberg, *Crit. Care Med.* **37**, 666 (2009).
- ¹⁶M. C. Kung, J.-K. Lee, H. H. Kung, and L. F. Mockros, *ASAIO J.* **54**, 383 (2008).
- ¹⁷J.-K. Lee, M. C. Kung, H. H. Kung, and L. F. Mockros, *ASAIO J. NIH Public Access* **54**, 390 (2008).
- ¹⁸W.-I. Wu, N. Rochow, E. Chan, G. Fusch, A. Manan, D. Nagpal, P. R. Selvaganapathy, and C. Fusch, *Lab Chip* **13**(13), 2641–2650 (2013).
- ¹⁹H. Matharoo, M. Dabaghi, N. Rochow, G. Fusch, J. Brash, C. Fusch, and P. R. Selvaganapathy, *Biomicrofluidics* **12**, 014107 (2018).
- ²⁰A. D. Meyer, A. A. Wiles, O. Rivera, E. C. Wong, R. J. Freishtat, K. Rais-Bahrami, and H. J. Dalton, *Pediatr. Crit. Care Med.* **13**, e255 (2012).
- ²¹J. Byrnes, W. McKamie, C. Swearingen, P. Prodhan, A. Bhutta, R. Jaquiss, M. Imamura, and R. Fiser, *ASAIO J.* **57**, 456 (2011).
- ²²A. J. Thompson, L. H. Marks, M. J. Goudie, A. Rojas-Pena, H. Handa, and J. A. Potkay, *Biomicrofluidics* **11**, 024113 (2017).
- ²³D. M. Hoganson, J. L. Anderson, E. F. Weinberg, E. J. Swart, B. K. Orrick, J. T. Borenstein, and J. P. Vacanti, *J. Thorac. Cardiovasc. Surg.* **140**, 990 (2010).
- ²⁴T. Kniazeva, J. C. Hsiao, J. L. Charest, and J. T. Borenstein, *Biomed. Microdev.* **13**, 315 (2011).
- ²⁵J. A. Potkay, M. Magnetta, A. Vinson, and B. Cmolik, *Lab Chip* **11**, 2901 (2011).
- ²⁶D. M. Hoganson, H. I. Pryor, E. K. Bassett, I. D. Spool, and J. P. Vacanti, *Lab Chip* **11**, 700 (2011).
- ²⁷T. Kniazeva, A. A. Epshteyn, J. C. Hsiao, E. S. Kim, V. B. Kolachalama, J. L. Charest, and J. T. Borenstein, *Lab Chip* **12**, 1686 (2012).
- ²⁸K. M. Kovach, M. A. LaBarbera, M. C. Moyer, B. L. Cmolik, E. van Lunteren, A. Sen Gupta, J. R. Capadona, and J. A. Potkay, *Lab Chip* **15**, 1366 (2015).
- ²⁹T. Rieper, C. Muller, and H. Reinecke, *Biomed. Microdev.* **17**, 86 (2015).
- ³⁰A. A. Gimbel, E. Flores, A. Koo, G. García-Cardena, and J. T. Borenstein, *Lab Chip* **16**, 3227 (2016).
- ³¹K. A. Burgess, H. H. Hu, W. R. Wagner, and W. J. Federspiel, *Biomed. Microdev.* **11**, 117 (2009).
- ³²J. A. Potkay, *Lab Chip* **14**, 4122 (2014).
- ³³H. Lorenz, M. Despont, M. Fahrni, N. LaBianca, P. Vettiger, and P. Renaud, *J. Micromech. Microeng.* **7**, 121 (1997).
- ³⁴K. Haubert, T. Drier, and D. Beebe, *Lab Chip* **6**, 1548 (2006).
- ³⁵E. P. Rivers, D. S. Ander, and D. Powell, *Curr. Opin. Crit. Care* **7**, 204 (2001).
- ³⁶W. Tin, *Arch. Dis. Child. - Fetal Neonatal Ed.* **84**, F106 (2001).
- ³⁷O. Siggaard-Andersen, P. D. Wimberley, N. Fogh-Andersen, and I. H. Gøthgen, *Scand. J. Clin. Lab. Invest.* **48**, 7 (1988).
- ³⁸S. Vashisht, *Anaesthesia* **59**, 88 (2004).
- ³⁹J. M. Leung, L. R. Berry, A. K. C. Chan, and J. L. Brash, *J. Biomater. Sci. Polym. Ed.* **25**, 786 (2014).
- ⁴⁰J. M. Leung, L. R. Berry, H. M. Atkinson, R. M. Cornelius, D. Sandejas, N. Rochow, P. R. Selvaganapathy, C. Fusch, A. K. C. Chan, and J. L. Brash, *J. Mater. Chem. B* **3**, 6032 (2015).
- ⁴¹K. M. Kovach, J. R. Capadona, A. Sen Gupta, and J. A. Potkay, *J. Biomed. Mater. Res. A* **102**, 4195 (2014).